The Journal of Chemical Physics

Addressing global uncertainty and sensitivity in first-principles based microkinetic models by an adaptive sparse grid approach

Cite as: J. Chem. Phys. **148**, 034102 (2018); https://doi.org/10.1063/1.5004770
Submitted: 15 September 2017 • Accepted: 29 December 2017 • Published Online: 16 January 2018

Sandra Döpking, Craig P. Plaisance, Daniel Strobusch, et al.

Addressing global uncertainty and sensitivity in first-principles based microkinetic models by an adaptive sparse grid approach

Sandra Döpking,[1] Craig P. Plaisance,[2] Daniel Strobusch,[2] Karsten Reuter,[2] Christoph Scheurer,[2] and Sebastian Matera[1,a)]
[1]*Institute for Mathematics, Freie Universität Berlin, Arnimallee 6, D-14195 Berlin, Germany*
[2]*Chair of Theoretical Chemistry and Catalysis Research Center, Technische Universität München, Lichtenbergstraße 4, D-85747 Garching, Germany*

(Received 15 September 2017; accepted 29 December 2017; published online 16 January 2018)

In the last decade, first-principles-based microkinetic modeling has been developed into an important tool for a mechanistic understanding of heterogeneous catalysis. A commonly known, but hitherto barely analyzed issue in this kind of modeling is the presence of sizable errors from the use of approximate Density Functional Theory (DFT). We here address the propagation of these errors to the catalytic turnover frequency (TOF) by global sensitivity and uncertainty analysis. Both analyses require the numerical quadrature of high-dimensional integrals. To achieve this efficiently, we utilize and extend an adaptive sparse grid approach and exploit the confinement of the strongly non-linear behavior of the TOF to local regions of the parameter space. We demonstrate the methodology on a model of the oxygen evolution reaction at the Co_3O_4 (110)-A surface, using a maximum entropy error model that imposes nothing but reasonable bounds on the errors. For this setting, the DFT errors lead to an absolute uncertainty of several orders of magnitude in the TOF. We nevertheless find that it is still possible to draw conclusions from such uncertain models about the atomistic aspects controlling the reactivity. A comparison with derivative-based local sensitivity analysis instead reveals that this more established approach provides incomplete information. Since the adaptive sparse grids allow for the evaluation of the integrals with only a modest number of function evaluations, this approach opens the way for a global sensitivity analysis of more complex models, for instance, models based on kinetic Monte Carlo simulations. *Published by AIP Publishing.* https://doi.org/10.1063/1.5004770

I. INTRODUCTION

In recent years, we have seen an increasing interest in first-principles-based microkinetic models for surface reactivity.[1] In these approaches, an elementary reaction mechanism and the corresponding energetic information on adsorption energies and reaction barriers are derived from predictive-quality electronic structure calculations. Besides the possibility to reduce the number of resource-intensive experiments, this provides mechanistic insight without being biased by fitting an approximate model to experimental results. We are then able to predict the material's performance, e.g., the turnover frequency (TOF, product molecules per active site and time) of a catalyst, and can address questions which cannot be answered solely on the basis of experimental data.[2–6]

However, in practice, first-principles electronic structure theory calculations have to rely on some intrinsic approximations to arrive at tractable computational costs. The resulting energetics then necessarily contain some error. For extended systems like solid surfaces, the most accurate methods that are presently still feasible are based on Density Functional Theory (DFT) in the generalized gradient approximation. Errors in the energetics for this class of density functionals are commonly believed to be around 0.2 eV.[1] Especially in low to intermediate temperature catalysis, this energetic uncertainty leads to sizable errors in the rate constants, i.e., at room temperature, the rate constants might be wrong by a factor 10 000. In principle, this uncertainty could fully propagate to the central observables of microkinetic modeling like TOF or surface coverages.

Large impacts of DFT errors have indeed been reported in the literature.[7–10] However, in general, we do not know the uncertainty of the microkinetic model output. Correspondingly, we are faced with corollary questions like which qualitative conclusions can still be drawn from the model? Or which uncertainties in the input energy parameters (mostly) affect the results? Answering the latter question would allow for selective refinement of the model by determining the corresponding input parameters with higher accuracy, either by employing a higher-level electronic structure theory (such as hybrid DFT functionals or embedded wave function approaches[11,12]) or by resorting to experimental data. In the context of computational materials screening, such information would also help us to identify descriptors for the material's performance. As the parameters entering a microkinetic model typically have an atomistic interpretation, this sensitivity information additionally provides important mechanistic insights into the details of the catalytic operation. For instance, the concept of rate-determining steps is directly linked to sensitivity analysis.[13,14]

a)Electronic mail: matera@math.fu-berlin.de

Most prevalent approaches for assessing the importance of parameters are based on local sensitivity analyses, i.e., on the derivatives of the model response with respect to the parameters.[13,15,16] However, microkinetic models are usually highly non-linear and the DFT uncertainty is not small. Thus, derivative-based approaches assuming linear behavior are likely to assign incorrect importance to the parameters. This is even more severe when one considers that the local sensitivity can easily change from zero to some sizable value within reasonable variations of the input parameters.[8,10,16] Therefore, global approaches that can fully account for non-linearities are required to obtain a meaningful sensitivity analysis.

In this study, we present an approach to such a global sensitivity analysis using adaptive sparse grids.[17] Specifically, we address the so-called total sensitivity index and the related Analysis Of Variance (ANOVA) decomposition.[18,19] This kind of sensitivity analysis has the benefit that the sensitivity measures have the interpretation of an induced uncertainty. Furthermore, it does not require any derivative information. Therefore, it is also directly applicable to models for which it is not possible, or at least very cumbersome, to obtain this kind of information, e.g., kinetic Monte Carlo models.[20]

Sparse grids (SGs) have recently gained popularity in the context of uncertainty and sensitivity analysis, mostly in the context of partial differential equation models.[21–23] This popularity results from the possibility to achieve high convergence rates even in higher dimensions, i.e., SGs are not so much affected by the curse of dimensionality. Being based on a basis set expansion, they also form a surrogate model of the underlying function and thereby also allow for the estimation of complex functional dependencies like the Total Sensitivity Index (TSI). This is particularly challenging for approaches based on Monte Carlo sampling of the parameter space, for which the most advanced approaches for estimating the TSI scale unfavorable with the number of relevant sensitivities.[19,24] These advantages of SGs come at the disadvantage that the classical sparse grid construction rules are only affordable in moderately high-dimensional parameter spaces. For microkinetic models with often dozens of elementary steps, adaptive grid refinement strategies are needed which exploit the properties of the investigated parameter response. For instance, we expect that only a subset of all parameters actually influence the response in a microkinetic model. Approaches exploiting this property are high-dimensional model representations[22] (also termed anchored ANOVA or, in the physics literature, multi-body expansion[25]), which try to represent the response as a sum of low-dimensional functions. An alternative is dimension adaptive SG,[26] which additionally adjusts the degree of resolution for each dimension. Also, we would expect that highly non-linear behavior appears only locally and therefore local refinement is desirable.[27] To exploit both properties, Jakeman and Roberts[23,28] have combined local and dimension adaptivity. We have modified this approach in order to allow for a larger number of parallel kinetic model evaluations and employ this throughout the study.

We demonstrate our approach on a recently developed model of the electrochemical oxygen evolution reaction (OER) on cobalt(II,III) oxide.[29,30] This material has received a significant attention recently as a low-cost and earth-abundant catalyst for the OER, which is the reaction that is responsible for most of the overpotentials required for electrocatalytic or photocatalytic water splitting.[31,32] We specifically investigate the active site on the (110)-A termination that consists of two redox-active Co cations sharing a bridging oxo species. For this system, we examine the sensitivity of the catalytic activity with respect to all energetic parameters of the model at room temperature and at varying applied potential. We find that the local sensitivity analysis tends to severely overestimate the impact of certain parameters, while other globally more important parameters are completely missed out by only considering derivative information. Still, we find that overall only a small subset of parameters controls the activity at a given overpotential. However, we also find that this subset changes significantly within the range of applied overpotentials.

The manuscript is organized as follows: In Sec. II, we shortly explain the model for the OER. We then continue with a summary of the basic concept of uncertainty and sensitivity analysis in Sec. III. The adaptive SG methodology is outlined in Sec. IV. Our results for the OER are presented in Sec. V, where we focus on three representative values for the overpotential and investigate the sensitivity of the TOF.

II. OXYGEN EVOLUTION ON THE COBALT(II,III) OXIDE (110)-A SURFACE

We consider the oxygen evolution on the Co_3O_4 (110)-A surface, employing the model presented in Refs. 29 and 30. We have chosen this model due to its easily comprehensible analytical form, which makes it perfectly suited for a demonstrator application of global sensitivity analysis and the SG approach.

The OER reaction mechanism at arbitrary applied potentials on the (110)-A surface of Co_3O_4 can be described by a general mechanism consisting of two irreversible non-electrochemical steps: (1) O–O bond formation by nucleophilic addition of water to a bound oxo species to form a bound hydroperoxo and (2) elimination of a bound superoxo as O_2 followed by adsorption of water on the resulting vacancy,[30]

$$H_2O + O\text{–}S_a(H_x)\text{–}O \rightarrow HO\text{–}S_a(H_x)\text{–}OOH, \quad \{1\}$$

$$H_2O + O\text{–}S_a(H_x)\text{–}OO \rightarrow HO\text{–}S_a(H_x)\text{–}OH + O_2. \quad \{2\}$$

Here, $Y\text{–}S_a(H_x)\text{–}X$ represents an arbitrary state of the active site S_a to which species X and Y are bound, with $0 \leq x \leq 12$ being the number of hydrogen atoms on the surface (as hydroxyl species). Of these two steps, only the O–O bond formation reaction is kinetically relevant. Between reactions {1} and {2}, the active site exists in a quasi-equilibrated ensemble of states $A_i = H_yO\text{–}S_a(H_x)\text{–}OOH_z$, with $y, z = 0, 1$. Likewise, the active site exists in a quasi-equilibrated ensemble of states $B_i = H_yO\text{–}S_a(H_x)\text{–}OH_z$ (also with $y, z = 0, 1$) between reactions {2} and {1}. The states in each ensemble are connected by quasi-equilibrated electrochemical reactions involving the coupled transfer of electrons to the bulk electrode and protons

to the bulk electrolyte,

$$A_i \rightleftharpoons A_j + (n_j - n_i)(H^+ + e^-), \quad \{3\}$$

$$B_i \rightleftharpoons B_j + (n_j - n_i)(H^+ + e^-), \quad \{4\}$$

where $n_i = 14 - x - y - z$ is the *degree of oxidation* of the state A_i or B_i, varying from 0 to 14. The degree of oxidation of state A_i or B_i is defined as the number of protons and electrons (only neutral surfaces are considered) that must be removed to obtain this state from a reference state A_0 or B_0. The electrons are removed from each of the 12 Co(III) cations in the surface layer, oxidizing them to Co(IV) (the final two are removed from surface oxygens). Reactions {3} and {4} are assumed to be quasi-equilibrated due to the typically low activation barriers of proton/electron transfer processes.[33] Since reaction {2} is irreversible and kinetically irrelevant, it is only necessary to consider reactions {1} and {3} in a kinetic model.

Since reaction {1} is the only kinetically relevant step in the catalytic cycle, the TOF is equal to the total rate of this reaction. There are several transition states TS_i through which reaction {1} can occur, each corresponding to one of the intermediate states A_i. The TOF is given as the sum of the rates r_i of this reaction through all such transition states TS_i,

$$\mathrm{TOF} = \sum_i r_i = \sum_i k_i \theta_i, \quad (1)$$

where k_i is the rate constant for reaction {1} proceeding from A_i through TS_i, and θ_i is the probability of the system being in intermediate state A_i. According to the transition state theory, the rate constant is given as

$$k_i = \frac{k_B T}{h} \exp\left(-\frac{G_{\mathrm{act},i}}{k_B T}\right), \quad (2)$$

with T being the temperature, while θ_i is given by the Boltzmann distribution,

$$\theta_i = \frac{\exp\left(-\frac{G_{\mathrm{int},i} - n_i e\eta}{k_B T}\right)}{\sum_j \exp\left(-\frac{G_{\mathrm{int},j} - n_j e\eta}{k_B T}\right)}. \quad (3)$$

The activation free energy $G_{\mathrm{act},i}$ is defined as the difference in free energy between the transition state TS_i and the intermediate state A_i. The quantity $G_{\mathrm{int},i}$ is defined as the free energy of intermediate state A_i with respect to the reference state A_0, with the free energy of a proton/electron pair taken with respect to the equilibrium potential of the OER at standard conditions (1.23 V vs. SHE). The term $-n_i e\eta$ appearing in the exponentials in Eq. (3) accounts for the changes in the free energies of the intermediate states as the applied electrochemical potential deviates from the OER equilibrium potential; this deviation is the applied overpotential η, and e is the unit of electronic charge.

The particular kinetic model that we employ considers a single intermediate state, the one with the lowest free energy, for each degree of oxidation from 0 to 14. These states are labeled with the index $i = 0, \ldots, 14$ equal to the degree of oxidation. In the kinetic model in Ref. 30, pathways for reaction {1} are considered from intermediate states 4, 6, 8, 10, and 12. These activation free energies, along with the free energies of the intermediate states, are given in Table I. For the most of this study, we will concentrate on this model. However, the reaction pathways from odd-numbered states 5, 7, 9, 11, and 13 are also possible, with similar activation barriers as for the even-numbered states. They were not included in the original model in Ref. 30 because, at the nominal parameter settings, the odd-numbered intermediate states are not significantly populated over the range of conditions that were examined. When varying the energies within reasonable bounds, this situation could change, and we will address the addition of the pathways from odd-numbered states in the discussion.

The nominal intermediate free energies $G_{\mathrm{int},i}$ and activation barriers $G_{\mathrm{act},j}$ (of the even-numbered states) are taken from Ref. 30, where these have been determined using Density Functional Theory (DFT) with a + U correction[34–36] applied to the Co 3d electrons. The $+U$ correction is necessary because the typically used semi-local exchange-correlation functionals over-delocalize the 3d electrons due to a spurious self-interaction error.[37] The DFT + U method requires the specification of an effective on-site Coulomb interaction U, which leads to some ambiguity in the method as there is no widely agreed-upon technique for determining its value. This leads to an increased uncertainty in the resulting energetics, which we take into consideration during the sensitivity analysis by employing a higher value of the uncertainty. We refer to Ref. 30 for a more complete discussion of this aspect.

Figure 1 shows the TOF obtained from this model as a function of the applied overpotential η. The temperature is kept fixed to 298.15 K and all energies were set to their nominal values. Below an applied overpotential of $\eta \approx 0.7$ V, the TOF increases exponentially with increasing η. Above this value, the TOF remains relatively constant around a value of approximately 10^3 s^{-1}. At applied overpotentials above 1.1 V, the TOF begins to rapidly decrease with overpotential. This decrease however may not be physical, as it arises from the absence of a reaction pathway in the kinetic model from the highly

TABLE I. Intermediate energies and activation barriers for the model for oxygen evolution on the Co_3O_4 (110)-A surface, taken from Refs. 29 and 30.

Intermediate energies		Activation energies	
$G_{int,0}$	0.00 eV	...	...
$G_{int,1}$	0.44 eV	...	...
$G_{int,2}$	0.88 eV	...	...
$G_{int,3}$	1.64 eV	...	...
$G_{int,4}$	2.33 eV	$G_{act,4}$	0.60 eV
$G_{int,5}$	3.09 eV	...	...
$G_{int,6}$	3.79 eV	$G_{act,6}$	0.59 eV
$G_{int,7}$	4.59 eV	...	...
$G_{int,8}$	5.38 eV	$G_{act,8}$	0.62 eV
$G_{int,9}$	6.22 eV	...	...
$G_{int,10}$	7.05 eV	$G_{act,10}$	0.60 eV
$G_{int,11}$	7.88 eV	...	...
$G_{int,12}$	8.71 eV	$G_{act,12}$	0.56 eV
$G_{int,13}$	9.77 eV	...	...
$G_{int,14}$	10.83 eV	...	...

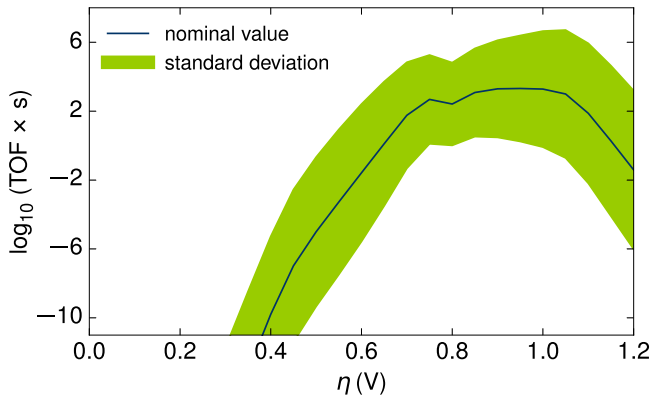

FIG. 1. Turnover frequency (TOF) as a function of the applied overpotential η for $T = 298.15$ K for the nominal energy values (blue line). The green area depicts the standard deviation of the model output by assuming uniformly distributed DFT-errors in a range of [−0.3, 0.3] eV (see the text).

oxidized surface state A_{14} which is present at high applied overpotentials.

The kinetic model just described has two types of input parameters: external reaction conditions, i.e., overpotential η and temperature T, and the material parameters $G_{\mathrm{int},i}$ and $G_{\mathrm{act},i}$. These material parameters can carry an error due to the approximate DFT functional used for determining them. The TOF curve should be complemented by error bars indicating the uncertainty of the model prediction due to the uncertainty in the energies. These error bars are represented by the green shaded area in Fig. 1, for which we have chosen the standard deviation (STD) of the logarithm of the TOF. The basic considerations behind such uncertainty analysis and the particular error model are discussed in the next Sec. III.

III. UNCERTAINTY AND SENSITIVITY ANALYSIS

The objective of uncertainty and sensitivity analysis is the quantification of the influence of parameter variations on the model response. For a deterministic input-output relation, we can write the model response $f : \mathbb{R}^D \mapsto \mathbb{R}$ as

$$y = f(x_1, x_2, \ldots, x_D), \tag{4}$$

where we use y to represent the output and $\vec{x} = (x_1, x_2, \ldots, x_D)$ to represent the inputs, and where D is the number of input parameters. In our case, the input parameters are the free energies of the intermediate states $G_{\mathrm{int},i}$ and the activation barriers $G_{\mathrm{act},j}$, and the output is the TOF, or more precisely the logarithm of the TOF (to base ten). That is, f results from inserting Eqs. (3) and (2) into Eq. (1). For more complex problems, the input-output relation might be only implicitly given by some computational model, e.g., by the numerical solution of microkinetic rate equations or by kinetic Monte Carlo simulations.

Additionally to the response, uncertainty and sensitivity analyses require a model of the parameter variation, i.e., a joint probability distribution on the D-dimensional parameter space usually given in terms of a probability density function (PDF) $p : \mathbb{R}^D \mapsto \mathbb{R}_0^+$,

$$p(x_1, x_2, \ldots, x_D). \tag{5}$$

The PDF p might represent the statistical errors in parameters, which originate from experiment. If obtained directly from independent experiments, the PDF is often taken as a product of Gaussian distributions with means and standard deviations adjusted to the experimental findings. By contrast, the DFT error is not statistical but systematic, resulting from the use of a necessarily approximate functional. Repeating the computational experiment will not lead to improved parameter estimates. The PDF must therefore be interpreted in an information theoretical sense. It reflects our knowledge about the possible outcomes of the parameters. For constructing the PDF, we follow the common assumption that DFT energies carry an uncertainty of ~0.2–0.3 eV.[1] Considering the somewhat larger uncertainty in the DFT + U method used for calculating the energetics, we would therefore expect that an upper bound for the errors would be in the range of 0.3 eV. A similar value was also deduced in Ref. 29 by comparison with more accurate correlated wave function calculations. Based on this limited knowledge, information theory yields that the energy parameters are uniformly distributed on the hypercube $\Omega = \vec{x}_{\mathrm{nom.}} + [-0.3\,\mathrm{eV}, 0.3\,\mathrm{eV}]^D$, centered at the nominal parameter settings $\vec{x}_{\mathrm{nom.}}$ (compare Table I),

$$p(\vec{x}) = \begin{cases} \dfrac{1}{(0.6\,\mathrm{eV})^D} & \text{if } \vec{x} \in \Omega \\ 0 & \text{else} \end{cases}. \tag{6}$$

This PDF maximizes the entropy among all PDFs which obey the bound constraints, i.e., we minimize the information content of the PDF. In reality, the errors of a particular DFT functional might show a trend for a certain class of materials, e.g., overbinding. Also there might be a certain degree of correlation, e.g., Brønsted-Evans-Polanyi relations might approximately apply.[38] However, in the lack of more detailed information, we here consider the worst case scenario, with completely uncorrelated errors, and employ no other information on the errors than the bounds. Constructing a more detailed PDF for DFT energetics is a cumbersome task[8,9,39] and beyond the scope of this study.

Having a PDF, we can now estimate the mean $E(y)$ and the variance $V(y)$ of the output

$$\begin{aligned} E(y) &= \int f(\vec{x}) p(\vec{x}) dx^D, \\ V(y) &= \int (f^2(\vec{x}) - E(y))^2 p(\vec{x}) dx^D, \end{aligned} \tag{7}$$

where the latter serves as a measure of the uncertainty. The green shaded area in Fig. 1 indicates the resulting standard deviation (STD) $\sigma = \sqrt{V(y)}$ for the TOF of the OER model and the outlined PDF (6), where $y = \log_{10}$ TOF. With our error model, i.e., our choice of the PDF, the STD for $\log_{10}$ TOF is between three and five, i.e., the TOF could, in principle, be five orders of magnitude larger or smaller than the nominal TOF obtained from the model. The difference of the mean $E(y)$ and the nominal $\log_{10}$ TOF values can be as large as two (i.e., two orders of magnitude). However, we have refrained from displaying the mean. The "true" curve will be obtained from a certain set of parameters and cannot be deduced by statistical averaging as the uncertainty of y cannot be regarded as fluctuation.

Other statistical quantities, like covariances between different model outputs, might provide additional information. In the following, we focus on the variance and its decomposition into contributions of each individual (energy) error. Such decomposition will provide us with the information, on which parameters the response depends sensitively. Combined with the atomistic interpretation of the parameters, this allows us to deduce which microscopic aspects are likely to control the catalytic activity taking into account that our parameters might be uncertain. If the PDF is in product form $p(x_1, x_2, \ldots, x_D) = p_1(x_1) \times p_2(x_2) \times \cdots \times p_D(x_D)$, i.e., the errors are statistically independent, and if we can safely assume a linear dependence of the response $f(\vec{x})$ on the parameters $\vec{x}$, the variance naturally decomposes into contributions of the different parameters

$$V(y) = \sum_i S_{i,\mathrm{LSA}} \quad \text{with} \quad S_{i,\mathrm{LSA}} = |\frac{\partial f}{\partial x_i}(\vec{x}_{\mathrm{nom.}})|^2 V(x_i), \tag{8}$$

where $V(x_i)$ is the variance of x_i.

The decomposition (8) is the motivation behind Local Sensitivity Analysis (LSA). The local sensitivity index $S_{i,\mathrm{LSA}}$ provides that part of the variance which is caused by the uncertainty of parameter x_i and therefore measures the importance of the uncertainty of x_i in this linear setting. If the derivative with respect to x_i and the uncertainty (the variance) of x_i are small, $S_{i,\mathrm{LSA}}$ will be small and the uncertainty of x_i is not very important. If both are large, $S_{i,\mathrm{LSA}}$ will be large and the uncertainty of x_i has a large impact. For all other cases, the balance between (local) dependence of $f(\vec{x})$ on x_i and the corresponding error will determine the local sensitivity index. Specifically, if $f(\vec{x})$ is locally independent of x_i, or x_i has very small variance, $S_{i,\mathrm{LSA}}$ will be close to zero and improving on the accuracy of x_i does not lead to any improvement in the model output.

However, LSA assumes a linear dependence. For a generally nonlinear response $f(\vec{x})$, LSA provides therefore only good estimates on the importance of errors for small parameter uncertainties. As might be expected from the results on the uncertainty in Fig. 1, 0.3 eV is far off from being small. In order to overcome the limitations of the LSA, Global Sensitivity Analysis (GSA) approaches are therefore appealing (see Ref. 18 for an overview). Here, we will specifically focus on the variance based methods, which allow us to interpret the sensitivity measures in terms of an induced uncertainty and for which there exist an easily comprehensible connection between GSA and LSA. The non-linear equivalent to the decomposition Eq. (8) is the so-called Analysis Of Variances (ANOVAs).[19] That is, given a product PDF $p(x_1, x_2, \ldots, x_D) = p_1(x_1) \times p_2(x_2) \times \cdots \times p_D(x_D)$, we can decompose f into a sum of functions with increasing dimensionality of the respective argument

$$f(\vec{x}) = f_0 + \sum_i^D f_{1,i}(x_i) + \sum_{i=1}^D \sum_{j,j>i}^D f_{2,ij}(x_i, x_j) + \cdots + f_D(\vec{x}), \tag{9}$$

where the terms $f_0, f_{1,i}, f_{2,ij}$, etc., are pairwise orthogonal, with respect to the scalar product $(f, g) = \int f g p dx^D$. Therefore f_0 is the mean and all other $f_{1,i}, f_{2,ij}$, etc., have a mean of zero. Equation (9) and the orthogonality also imply the decomposition

$$V(y) = \sum_i^D V_{1,i} + \sum_{i=1}^D \sum_{j,j>i}^D V_{2,ij} + \cdots + V_D \tag{10}$$

of the variance, where the contributions $V_{1,i}, V_{2,ij}$, etc., are the variances of the corresponding terms $f_{1,i}, f_{2,ij}$, etc., in Eq. (9). As mentioned, the ANOVA relies on a product PDF. Extensions for more general PDFs exist;[40,41] however, our error model, Eq. (6), is a product PDF. The ANOVA decomposition, Eqs. (9) and (10), allows us to address the impact of the parameter x_i. Only the terms $f_{1,i}, f_{2,ij}$, etc., where i appears in the index, actually depend on x_i and only the corresponding contributions $V_{1,i}, V_{2,ij}$, etc., will therefore be affected by the uncertainty of x_i. The contribution $V_{1,i}$ is called the first order index (also termed the main effect) and $V_{2,ij}$ are second order indices representing the "interaction" between two parameters and so on. If all but the first order effects are zero, the function can be represented as a sum of one-dimensional functions and we arrive at a similar decomposition as in the case of LSA. If $f(\vec{x})$ is linear, $S_{\mathrm{LSA},i}$ and $V_{1,i}$ will agree.

The number of variance contributions $V_{i<j<k\cdots}$ grows exponentially fast with the dimension D. For large D, an ANOVA not only challenges the computational resources but also the myriad of resulting numbers makes an interpretation difficult. In addition, we are only interested in the effective impact of the uncertainty of the parameters $\vec{x}$ and not in all the details of their interaction. However, considering only the first order effects V_1 is not sufficient because significant portions of the output variance might result from higher order effects. In fact, the first order effect $V_{1,i}$ might be zero, even though the parameter x_i has a large impact. Not withstanding, if we sum over all ANOVA terms in which x_i appears, we will account for all possible interactions. This leads to the Total Sensitivity Index (TSI)[42]

$$\begin{aligned} S_{\mathrm{T},i} &:= V_{1,i} + \sum_{j\neq i} V_{2,ij} + \cdots + V_D \\ &= E(V(y|\vec{x}_{\sim i})). \end{aligned} \tag{11}$$

Here we omitted the common normalization with the total variance V[18,19,42] because we want to compare LSA and GSA sensitivities in the context of induced uncertainty. $V(y|\vec{x}_{\sim i}))$ is the variance which results from varying x_i when we fix all other parameters, i.e., it is a function of the remaining parameters $\vec{x}_{\sim i}$. The TSI $S_{\mathrm{T},i}$ is therefore the resulting variance, if only x_i would be uncertain, averaged over all other parameters. In other words, the TSI allows for the targeted interpretation of an induced uncertainty. Yet, in general, nonlinear setting, the TSIs are not a decomposition of the total variance, as their sum can be larger. Only in the case, when the function f is a sum of only one-dimensional functions, the TSIs sum up to the total variance and an interpretation as for Eq. (8) can strictly be made. In this case, TSI and the first order effect agree, and, for linear f, $S_{i,\mathrm{LSA}}$, and $S_{\mathrm{T},i}$ will therefore agree.

IV. SPARSE GRIDS

Unlike the linear case, the variance and the TSI need to be obtained by averaging over the parameter distribution. For reaction models with often dozens of elementary

reactions and corresponding ΔG_i, this requires the solution of high-dimensional integrals. This integration needs to be performed numerically, as analytic solutions might not be available or, in the general case, the response is only implicitly given by some simulation. The prevalent approaches for such high-dimensional integration are Monte Carlo or quasi Monte Carlo methods. Here, we follow a different route using sparse grids (SGs),[17] which offer a number of advantages like higher convergence rates or the construction of a surrogate model. Specifically the estimation of the ANOVA decomposition and the TSI can be performed efficiently from a given SG expansion, while Monte Carlo approaches for this scale unfavorably with the dimension.[19,24]

As classical full grid approaches, SGs solve the integration problem by constructing a D-dimensional interpolation based on products of one-dimensional basis functions. The difference is that the SG approach omits "higher order cross-terms" and the corresponding grid points, which do not increase the accuracy. Thereby, it reaches a convergence of $\mathcal{O}(N^{-r}(\log N)^{r(D-1)})$ with the number of grid points N, when the underlying one-dimensional formula has a convergence of $\mathcal{O}(N^{-r})$. It thus overcomes the curse of dimensionality of the classical approaches which converge as $\mathcal{O}(N^{-r/D})$, i.e., very slowly for high-dimensional problems.

In this study, we adopt a local and dimension-adaptive SG approach using locally supported piecewise linear basis functions. We expect this approach to be particularly suited for our purpose. First, we expect that we will have only significant variability of the TOF in just a few directions (dimension adaptivity). Second, in the logarithmic representation for the TOF, we also expect an almost linear behavior for the largest parts of the parameter space, which implies the use of piecewise linear basis functions. These domains of almost linear behavior are connected by narrow regions where the TOF changes rapidly (local adaptivity). It is due to this latter property, why we also refrain from employing higher order basis functions to avoid artificial oscillation close to the regions of rapid change.

As the employed h-adaptive Generalized Sparse Grids (h-GSGs) have been detailed by Jakeman and Roberts,[23,28] we only provide a coarse overview of the method and the main ideas behind the method and our modifications. For this, we assume that we can find a coordinate transformation such that the parameters are uniformly distributed on $[-0.5, 0.5]^D$. This is definitely possible for the PDF (6), but also many other PDFs allow for such a transformation.

A. Hierarchical basis and sparse grid construction

The starting point for the approach is a one-dimensional interpolation rule, i.e., we approximate a given one-dimensional function $f(x)$ with

$$f(x) \approx u(x) = \sum_i \nu_i \varphi_i(x), \tag{12}$$

where the basis functions (BFs) φ_i are given and the expansion coefficients ν_i are determined by the interpolation requirement $u(x_i) = f(x_i)$ for some given grid points x_i. Usually, the grid points are determined by the choice of the basis and each BF corresponds to a certain x_i. For an adaptive interpolation (and quadrature), we employ a so-called hierarchical basis.

The idea behind hierarchical bases is to start with a coarse resolution (i.e., low number of grid points) and the basis functions which would lead to a, in our case, piecewise linear interpolation between these points. If we now find that the function is not well represented, we keep the old BFs, add new points, and then add only those new BFs which are needed to interpolate the refined set of points.[17,27] The new BFs thus only interpolate the difference between the coarse and the refined interpolation. If the refined interpolation is still too bad, we can proceed in the same way. We repeat this until two subsequent interpolations show only a reasonably small difference, i.e., the new BFs will have only a small contribution in the basis set expansion of the original function. The space W_{l+1} spanned by the BFs added during the $(l+1)$-th refinement can thus be regarded as the refinement of the space W_l spanned by the BFs added in the refinement step before. In the following, we will call the number of refinements l needed to reach a certain resolution, the *level index*. For brevity, we also use it to identify the set of BFs added in the lth refinement. In the following, we use the abbreviation parent (level) and child (level) for levels l and $l+1$. Of course, every level usually contains a number of BFs and corresponding grid points. We identify these by providing their level index l and a *count index* i and write $\varphi_{l,i}$ for a BF and $x_{l,i}$ for the corresponding grid point.[43,44] In practice, we employ the basis set depicted in the left panel of Fig. 2. The BFs are defined by[45]

$$\varphi_{l,i}(x) := \begin{cases} 1 & \text{for } l = 0 \\ \max(1 - 2^{l-1}|x - x_{l,i}|, 0) & \text{for } l > 0 \end{cases} \tag{13}$$

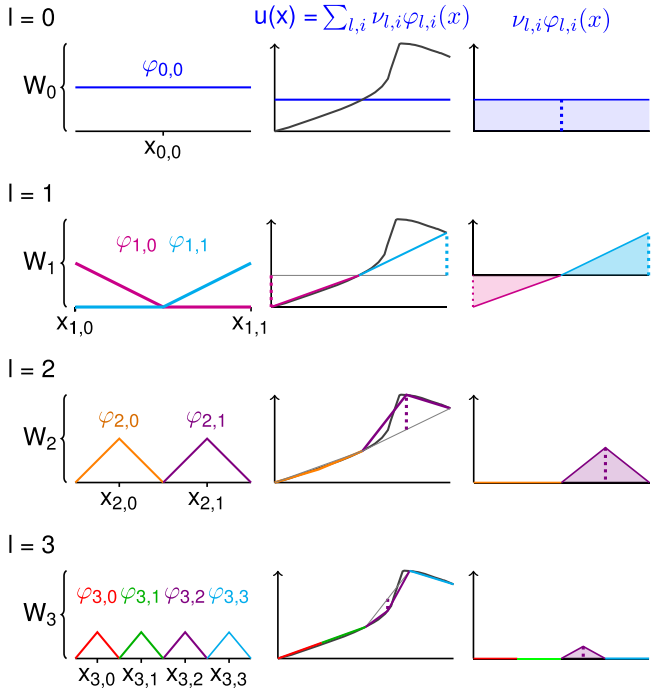

FIG. 2. Illustration of the hierarchical interpolation in one dimension with increasing level index. Left: Basis functions added at the corresponding levels l. Middle: The original function $f(x)$ and the hierarchical interpolation $u(x) = \sum_{l,i} \nu_{l,i}\varphi_{l,i}(x)$. Right: Illustration of the contribution of the basis functions added at each level $\nu_{l,i}\varphi_{l,i}(x)$. The contributions decrease with increasing level, and, at the finest level, only those basis functions close to the sharp non-linearity still have significant contributions to the interpolation.

with $x_{0,0} = 0$, $x_{1,0/1} = \mp 0.5$, $x_{2,0/1} = \mp 0.25$, and $x_{l,i} = x_{l-1,\lfloor i/2 \rfloor} - (-1)^i/2^l$. This choice of the basis dictates the following refinement strategy. At $l = 0$, we have only a single constant BF and the corresponding grid point $x_{0,0}$ is in the center of the interpolation interval. For $l = 1$, the points $x_{1,0}$ and $x_{1,1}$ on the boundary need to be created. The corresponding BFs decay linearly towards the midpoint and are zero afterwards. For every higher level, new grid points are created in the center between two existing points. The BFs take the value 1 at these new points, decay linearly towards neighboring (old) grid points, and are zero outside this interval. If we add all points up to a level l, we end up with a linear interpolation on $2^{l+1} + 1$ equidistant grid points. An important property of this hierarchical basis is thereby that the support of $\varphi_{l,i}(x)$ is covered only by $\varphi_{l+1,2i}(x)$ and $\varphi_{l+1,2i+1}(x)$. Therefore any improvement on the interpolation on this interval must come from these two basis functions and thus $\varphi_{l+1,2i}(x)$ and $\varphi_{l+1,2i+1}(x)$ somewhat refine $\varphi_{l,i}(x)(l > 1)$. We therefore have a parent-child relation not only for level indices but also for BFs and corresponding grid points.

The behavior of this hierarchical basis during refinement is depicted in Fig. 2 for the refinement levels $l = 0$ to $l = 3$. The left panel shows the BFs added at each refinement level. The middle panel shows the target function and the interpolation. The right panel displays the contributions from the added BFs (the expansion coefficient times the BF). When refining from $l = 1$ to $l = 2$, most of the new BFs have an almost zero contribution except $\varphi_{2,1}$, and the interpolation captures the main characteristics of the original. The functions from $l = 3$ have therefore only vanishing or very small contribution. Indeed, $\varphi_{3,0}$ and $\varphi_{3,1}$ could have been neglected and we could have seen this in advance as their parent $\varphi_{2,0}$ already did not contribute much. An adaptive refinement would therefore proceed as follows: in the first step, we add all grid points and basis functions up to a level l_0. We then look at the basis functions with the highest level index and, if their expansion coefficient is above a predefined threshold, we add their child functions and corresponding grid points. We then proceed in the same way for the BFs we have just added. We repeat this until we find no BFs above our threshold.

If we deal with D-dimensional functions on a hypercube, we employ the product BFs resulting from the one-dimensional basis

$$\varphi_{\vec{l},\vec{i}}(\vec{x}) = \prod_{j=1}^{D} \varphi_{l_j,i_j}(x_j). \tag{14}$$

The level $\vec{l}$ and count index $\vec{i}$ have become D-dimensional integer vectors, with the one-dimensional level and count indices for each direction as entries. A SG interpolation is then obtained by the expansion

$$\begin{aligned} u(\vec{x}) &= f_0 + \sum_{|\vec{l}|_1=1,\vec{i}} v_{\vec{l},\vec{i}}\varphi_{\vec{l},\vec{i}}(\vec{x}) + \sum_{|\vec{l}|_1=2,\vec{i}} v_{\vec{l},\vec{i}}\varphi_{\vec{l},\vec{i}}(\vec{x}) \dots \\ &= \sum_{|\vec{l}|_1 \le l_{\max},\vec{i}} v_{\vec{l},\vec{i}}\varphi_{\vec{l},\vec{i}}(\vec{x}), \end{aligned} \tag{15}$$

where the expansion coefficients $v_{\vec{l},\vec{i}}$ are also called the hierarchical surplus. In Eq. (15), only those BFs (and grid points) are employed, for which the 1-Norm of the level index $\vec{l}$ (the sum over all entries) does not exceed a predefined maximum refinement level l_{max}. This is in contrast to the full grid approach where all combinations of 1D BF up to a maximum refinement l_{max} are used for the interpolation. In Eq. (15), this would simply mean replacing the 1-norm $|\cdot|_1$ with the maximum norm $|\cdot|_\infty$. By the choice of a maximum refinement level for all directions together, the SG strategy thus overcomes the curse of dimensionality.

Given the SG interpolant, we can now efficiently approximate expected values, variances, and the TSI. For the assumed uniform distribution on $\Omega = [-0.5, 0.5]^D$, we have for the expected value

$$\begin{aligned} E(y) \approx \int_\Omega u(\vec{x})dx &= \int_\Omega \sum_{\vec{l},\vec{i}} v_{\vec{l},\vec{i}}\varphi_{\vec{l},\vec{i}}(\vec{x})\, dx^D \\ &= \sum_{\vec{l},\vec{i}} v_{\vec{l},\vec{i}} \underbrace{\int_\Omega \varphi_{\vec{l},\vec{i}}(\vec{x})\, dx^D}_{w_{\vec{l},\vec{i}}} = \sum_{\vec{l},\vec{i}} v_{\vec{l},\vec{i}} w_{\vec{l},\vec{i}}, \end{aligned} \tag{16}$$

where $w_{\vec{l},\vec{i}}$ is the integration weight attributed to the basis function $\varphi_{\vec{l},\vec{i}}(x)$. For the variance, we need to approximate the second moment, which we can compute from an existing SG as

$$\begin{aligned} E(y^2) \approx \int_\Omega u(\vec{x})^2 dx^D &= \int_\Omega \left(\sum_{\vec{l},\vec{i}} v_{\vec{l},\vec{i}}\varphi_{\vec{l},\vec{i}}(\vec{x}) \right)^2 dx^D \\ &= \sum_{\vec{l},\vec{i},\vec{l}',\vec{i}'} v_{\vec{l},\vec{i}} v_{\vec{l}',\vec{i}'} w_{\vec{l},\vec{i},\vec{l}',\vec{i}'}, \end{aligned} \tag{17}$$

where $w_{\vec{l},\vec{i},\vec{l}',\vec{i}'} = \int_{[-0,5,0.5]^D} \varphi_{\vec{l},\vec{i}}(\vec{x})\varphi_{\vec{l}',\vec{i}'}(\vec{x})dx^D$. Finally, we utilize the SG representation to estimate the TSI for the sensitivity with respect to the parameter x_α,

$$\begin{aligned} S_{T,\alpha} &\approx \int_{\Omega_{\sim\alpha}} \left(\int_{-0.5}^{0.5} u(\vec{x})^2 dx_\alpha \right) dx_{\sim\alpha}^{D-1} - \int_{\Omega_{\sim\alpha}} \left(\int_{-0.5}^{0.5} u(\vec{x}) dx_\alpha \right)^2 dx_{\sim\alpha}^{D-1} \\ &= \int_\Omega \left(\sum_{\vec{l},\vec{i}} v_{\vec{l},\vec{i}}\varphi_{\vec{l},\vec{i}}(\vec{x}) \right)^2 dx^D \\ &\quad - \int_{\Omega_{\sim\alpha}} \left(\int_{-0.5}^{0.5} \sum_{\vec{l},\vec{i}} v_{\vec{l},\vec{i}}\varphi_{\vec{l},\vec{i}}(\vec{x}) dx_\alpha \right)^2 dx_{\sim\alpha}^{D-1}, \end{aligned} \tag{18}$$

where $\int_{\Omega_{\sim\alpha}} \dots dx_{\sim\alpha}^{D-1}$ represents the integration over all variables except x_α. Exploiting the product form of the BFs (14), we arrive at

$$S_{T,\alpha} \approx \sum_{\vec{l},\vec{i},\vec{l}',\vec{i}'} v_{\vec{l},\vec{i}} v_{\vec{l}',\vec{i}'} \prod_{\beta\neq\alpha} w^\beta_{\vec{l},\vec{i},\vec{l}',\vec{i}'} (w^\alpha_{\vec{l},\vec{i},\vec{l}',\vec{i}'} - w^\alpha_{\vec{l},\vec{i}} w^\alpha_{\vec{l}',\vec{i}'}), \tag{19}$$

where

$$w^\alpha_{\vec{l},\vec{i}} = \int_{-0.5}^{0.5} \varphi_{l_\alpha,i_\alpha}(x)\, dx$$

and

$$w^{\beta}_{\vec{l},\vec{i};\vec{l}',\vec{i}'} = \int_{-0.5}^{0.5} \varphi_{l_\beta,i_\beta}(x)\varphi_{l'_\beta,i'_\beta}(x)\,dx.$$

Similar expressions can be derived for the first order, second order, etc., indices in the ANOVA decomposition.

B. Adaptivity

In addition to the potentially fast convergence, the SG approach also allows for adaptive refinement because the BFs, Eq. (14), inherit the hierarchical structure of the one-dimensional BFs, Eq. (12). As in the one-dimensional case, the space $W_{\vec{l}+\vec{e}_k}$, spanned by the BFs $\varphi_{\vec{l}+\vec{e}_k,\vec{i}}$, can be considered as a refinement of the space $W_{\vec{l}}$, where $\vec{e}_k$ is the unit vector in the kth direction. Analogously, the BF $\varphi_{\vec{l},\vec{i}}$ has two children in $W_{\vec{l}+\vec{e}_k}$.[23,28] The corresponding grid points are located at $x_{\vec{l},\vec{i}} \pm (h_{l_k}/2)\vec{e}_k$, where h_{l_k} is the grid spacing for the (one-dimensional) level index l_k, i.e., $h_{l_k} = 1/2^{l_k}$ for the considered interpolation domain $[-0.5, 0.5]^D$. A local adaption strategy could now be based on creating only the children of BFs whose surplus exceeds a certain threshold. However, one of the main characteristics of catalytic TOFs is rapid local changes with a large gradient, whose approximation has a slowly decreasing hierarchical surplus, while producing BFs with only limited contribution to the targeted integrals. We therefore employ the error criterion[22,28]

$$\gamma_{\vec{l},\vec{i}} := |v_{\vec{l},\vec{i}} w_{\vec{l},\vec{i}}|. \tag{20}$$

This avoids that the method refines too often, when the original function has characteristics that are close to behaving discontinuously. The locally (h-)adaptive strategy works as in the one-dimensional setting. We visit every grid point (BF) and calculate the criterion $\gamma_{\vec{l},\vec{i}}$ for every point. For those points, where $\gamma_{\vec{l},\vec{i}}$ exceeds a predefined threshold *tol*, we add the child points (and BFs) $x_{\vec{l},\vec{i}} \pm (h_{l_k}/2)\vec{e}_k, \forall k$ for all directions to the interpolation (if they do not already exist). On the basis of the now extended point set and function values, we create a new interpolant and repeat the refinement. We stop when no new points are identified in the refinement step.

The h-adaptive approach is in principle also dimension adaptive. Yet, it still creates children in every direction. For kinetic TOF data, where most directions require only a coarse resolution, most of these children will not contribute to an increase in accuracy. The Generalized Sparse Grids (GSGs) method[26] adaptively chooses which direction should be resolved finer. It is based on the following consideration: A given level index $\vec{l}$ is usually the child of multiple parent levels $\vec{l} - \vec{e}_k$ (max. D levels) and can be regarded as a refinement of all of them. If one of the parent levels $\vec{l} - \vec{e}_k$ has only small contributions to the SG interpolant $u(\vec{x})$, we do not need to add its children and thus we can omit the BFs and corresponding grid points from $\vec{l}$. In the original approach of Gerstner and Griebel, the GSG procedure selects the level $\vec{l}$ among the existing ones with highest contributions, measured by $\gamma_{\vec{l}} := \sum_{\vec{i}\in\vec{l}} \gamma_{\vec{l},\vec{i}}$. Then those child levels $\vec{l} + \vec{e}_k$ are selected for which all parents exist. As in the locally adaptive scheme, the grid points corresponding to BFs in these child spaces are then added to the interpolation. This is repeated until a predefined criterion is met. The GSG is not locally adaptive. To achieve this, the h-GSG combines it with the h-adaptive strategy by only adding the points, which have been proposed for refinement by both approaches.[23,28]

For this study, we have modified the h-GSG in order to allow for more parallel function evaluations, i.e., we do not only select a single level $\vec{l}$ but multiple levels in the level adaption. For this, we consider the (level) refinement criterion

$$\gamma_{\vec{l}} := \max_i \gamma_{\vec{l},\vec{i}}\,. \tag{21}$$

Then, we mark all existing levels l for refinement, for which $\gamma_{\vec{l}}$ is above the threshold *tol*. Those child levels $\vec{l} + \vec{e}_k$ are proposed to be added, for which all parent levels $\vec{l} + \vec{e}_k - \vec{e}_m$ meet the criterion $\gamma_{\vec{l}+\vec{e}_k-\vec{e}_m} > tol$. This dimension adaptive strategy is then combined with the h-adaptive approach, by adding only the intersection between the two proposed point sets in each refinement step. The refinement naturally stops, when the intersection is empty. The use of the maximum norm for the level refinement criterion allows us to employ the same threshold for both refinement strategies. Thus, in each refinement step, we add those grid points and BFs for which one parent BF has a $\gamma_{\vec{l},\vec{i}}$ above the refinement tolerance and for which there is at least one BF above the threshold in each parent level.

In the sparse grid setting, our (as well as the h-GSG and the GSG) approach can be regarded as a generalization of the multibody expansion approach (also called the anchored ANOVA or high-dimensional model representation).[22,25,46] As in ANOVA, these approaches represent the function of interest as a sum of functions with increasing dimensionality, albeit without the orthogonality constraint. The idea is to truncate the expansion at some point. Each of these functions is then independently interpolated, for instance, by h-adaptive SGs.[22,25] Thus all level indices l_i in one of these terms will have the same maximum $l_{\max}$, except those which correspond to the discarded dimensions in the respective term. The here employed dimension adaptivity, on the other hand, expands the function into terms with different resolutions for each direction, i.e., in one term of the anchored ANOVA, the maximum level indices are allowed to differ. This allows for a further reduction of the number of BFs compared to a multibody expansion.

We depict the dimension and local adaptivity for a function $f(x, y)$ in a two-dimensional system $\Omega = [-0.5, 0.5]^2$ in Fig. 3. The function is assumed to vary only for $x < 0$ and to be independent of y (seen in the middle panel). The SG method starts with an initial set of points, which would include 5 points, one central point and two additional ones for each dimension (upper left). A full SG would produce eight refinement points (red crosses) for the next step (upper right). The dimension adaptivity exploits that the impact of $l(0, 1)$ is zero because we have no variation in this direction, removing 6 of the potential candidates (circles, lower right). As the function only varies in the left half, the subsequent local adaptivity removes a further grid point, resulting in a single point that needs to be added (lower left). For the considered function, the surplus of the adaptively removed grid points

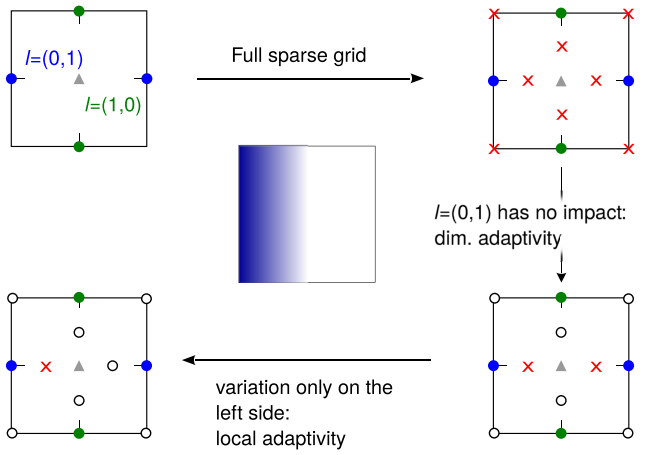

FIG. 3. Dimension and local adaptivity of the SG method for a two-dimensional space. The middle picture displays the function defined on the space $\Omega = [-0.5, 0.5]^2$ with variation only along the x-axis in the left half of the space and constant behavior in the right half. The refinement starts with an initial grid of 5 points (picture top left), one center point and two according to each level index. A full refinement step would produce 8 points (red crosses, top right), but the dimension adaption identifies no change along the y-axis and drops 6 points (black circle, bottom right). In the last step, the local adaptivity reduces the amount of points to 1, exploiting that the variation happens only in the left half of the domain.

would actually be zero as would be the case for all their child nodes.

In practice, the performance of any adaptive scheme relies on a sufficiently sampled initial grid, which resolves features well enough such that the adaptive strategy recognizes these and does not suffer from a too early termination. The initial grid of the above example would, for instance, be insufficient if the function would only vary in the upper left corner, while being zero everywhere else. This could be solved by employing a full SG of level two as starting point. However, trying to have a well enough resolved (full) SG as a starting point might soon become impractical in high dimensions. We therefore generate an initial grid by employing a very low threshold for the error of $tol = 10^{-5}$, while limiting the maximum norm of the level indices to one, $|l|_\infty = 1$. As a result, we include all interactions between the dimensions in the first refinement step (for each dimension). Hence, with this method, our initial grid already adapts to important features on a coarse level, which makes the subsequent SG algorithm more effective. This high accuracy is only needed for the adaptive algorithm to sufficiently explore the domain. Using the resulting grid as a starting point, the actual refinement without limitations of the level indices can then be performed with higher thresholds $tol \in = [10^{-1}, 10^{-3}]$. These then provide sufficient accuracy for the targeted statistical measures.

V. RESULTS

We now turn to a detailed analysis of the OER on the Co_3O_4 (110)-A surface termination, employing the nominal model where reaction {1} is only allowed to occur from even numbered states, cf. Sec. II. Specifically, we address the uncertainty and sensitivity of $\log_{10}$ TOF with respect to all 20 uncertain free energies $G_{\text{int},i}$ and $G_{\text{act},i}$ using the error model of Eq. (6), with a maximum error of 0.3 eV for each energy.

Choosing the logarithm instead of the linear TOF allows us to connect to the established local sensitivity measures of chemical kinetics,[13] which consider the derivatives of the logarithm. From a practical point of view, this makes the interpolation easier because we expect that $\log_{10}$ TOF has an almost piecewise linear behavior in most of the interpolation domains. Strong non-linear dependence is expected to appear only in narrow regions connecting kinetic regimes with different linear dependencies.

The top image in Fig. 4 shows the $\log_{10}$TOF as a function of the errors in $\Delta G_{\text{int},4}$ and $\Delta G_{\text{act},4}$ for $\eta = 0.7$ V and $T = 298.15$ K, while all other energies are fixed to their nominal values. Within the interpolation domain, the function shows three dominant regimes: (I) for medium to high $\Delta G_{\text{int},4}$ and $\Delta G_{\text{act},4}$, the response is independent of these two variables, (II) at low $\Delta G_{\text{int},4}$, the TOF depends only on $\Delta G_{\text{act},4}$, and (III) at low to medium $\Delta G_{\text{act},4}$ and high to medium $\Delta G_{\text{int},4}$, the derivative with respect to both energies is non-zero. In a smaller sub-domain IV (medium to low $G_{\text{int},4}$ and medium to high $G_{\text{act},4}$), the response solely depends on the intermediate energy. Within each of these regimes, $\log_{10}$ TOF behaves almost linear, as expected. The non-linear transitions (indicated by dotted lines in Fig. 4) between these regimes are not really sharp but still rather local. The bottom two images in Fig. 4 show the SG grid points in this two-dimensional

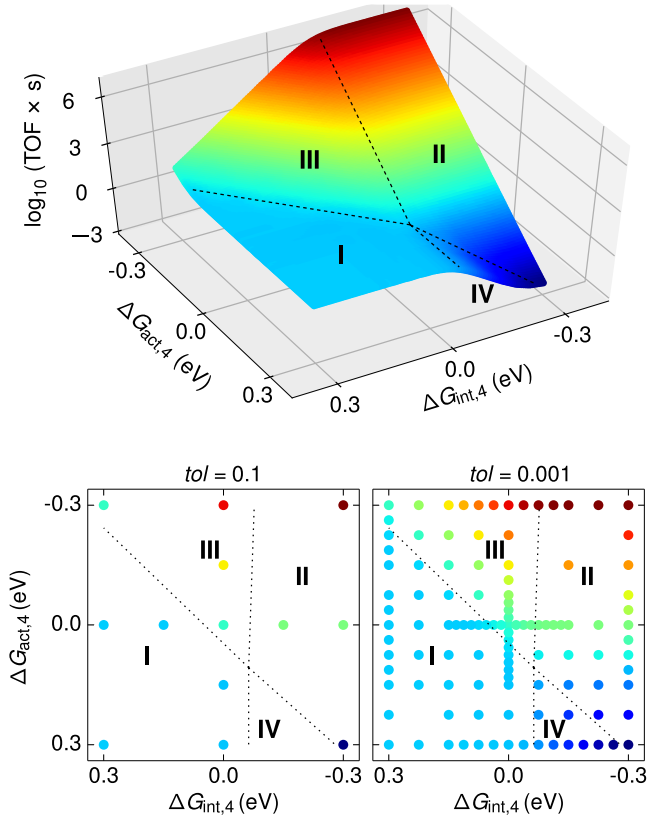

FIG. 4. Upper panel: Two-dimensional dependence of the turnover frequency on energy errors $\Delta G_{\text{int},4}$ and $\Delta G_{\text{act},4}$ at an overpotential of $\eta = 0.7$ V. The dotted lines indicate the borders between the four regimes: (I) no dependence on $\Delta G_{\text{int},4}$ and $\Delta G_{\text{act},4}$, (II) only depending on $\Delta G_{\text{act},4}$, (III) depending on both, and (IV) only depending on $\Delta G_{\text{int},4}$. Lower panel: Adaptive grid for two applied tolerances: $tol = 0.1$ (left) and $tol = 0.001$ (right). In the upper panel, dotted lines indicate borders between the four regimes. Refinement primarily happens close to the origin, where the four regimes meet.

plane from the full 20-dimensional adaptive interpolation. The left grid corresponds to a threshold of $tol = 0.1$, while the right grid was obtained by setting $tol = 0.001$. Refinement mostly happens close to the origin, where the four regimes meet.

For our analysis, we concentrate on three representative values for the overpotential η: (i) 0.4 V corresponding to the kinetic regime at low η where the TOF increases exponentially at nominal parameter settings, cf. Fig. 1, (ii) 0.7 V corresponding to the start of the kinetic regime at higher η where the TOF is relatively constant at nominal parameter settings, and (iii) 1.0 V corresponding to the end of this kinetic regime. For all three values of η, we obtain the initial grid from an adaptive run with very low $tol = 10^{-5}$ but fixed maximum resolution for each direction as described in Sec. IV B.

For these three values for the applied overpotential, we find the variances of $\log_{10}$(TOF) to be 20.9 ($\eta = 0.4$ V), 9.5 ($\eta = 0.7$ V), and 11.3 ($\eta = 1.0$ V). For the TOF, this corresponds to uncertainties between three and five orders of magnitude. Reasonably accurate estimates are already found for a refinement tolerance $tol = 0.1$ in the adaptive strategy. Reducing the tolerance to $tol = 0.001$ leads to only minor changes of these numbers. But, even for the latter tolerance, the number of grid points stays moderate, between 1000 ($\eta = 0.4$ V) and 14 000 ($\eta = 0.7$ V). Convergence tests with respect to tol for the expectation $E(\log_{10}\,\mathrm{TOF})$, the variance $V(\log_{10}\,\mathrm{TOF})$ and the sensitivities can be found in the supplementary material.

A. Sensitivity analysis

We now investigate which errors are responsible for the reported uncertainties. Figure 5 shows the TSIs for the three considered values of the overpotential η (top 0.4 V, middle 0.7 V, bottom 1.0 V). We also show the outcome of a LSA in order to address the impact of non-linearities and to scrutinize this more common approach to sensitivity analysis.[13] In each panel, the 20 input parameters are separated into the two different classes, intermediate free energies $G_{\mathrm{int},i}$ and activation free energies $G_{\mathrm{act},i}$. The gray-shaded areas correspond to the intermediate states from which no reaction pathway was considered in the kinetic model in Ref. 30, i.e., no corresponding $G_{\mathrm{act},i}$ is included in the kinetic model. Working on a logarithmic scale and with variances, the sensitivity indices might be interpreted as follows: a value of 1 corresponds roughly to a factor ten for the TOF induced by the respective parameter. A value of 4 corresponds to an induced STD of 2 for the $\log_{10}$(TOF) resulting in a multiplicative error of 100 on the linear scale for the TOF. Correspondingly, values of 0.5, 2 and 8 are responsible for multiplicative errors in the TOF of roughly 5, 25, and 700, respectively.

When comparing the three values of η, both LSA and GSA show a similar rough trend: at low η, parameters corresponding to states with low degrees of oxidation ($i < 5$) are most important and when increasing η, this importance shifts to states with higher degrees of oxidation. This corresponds to what we would expect from physical intuition. At low applied overpotential ($\eta < 0.4$ V), the system will predominantly exist in the state with the lowest degree of oxidation (A_0). All intermediate states with higher degrees of oxidation

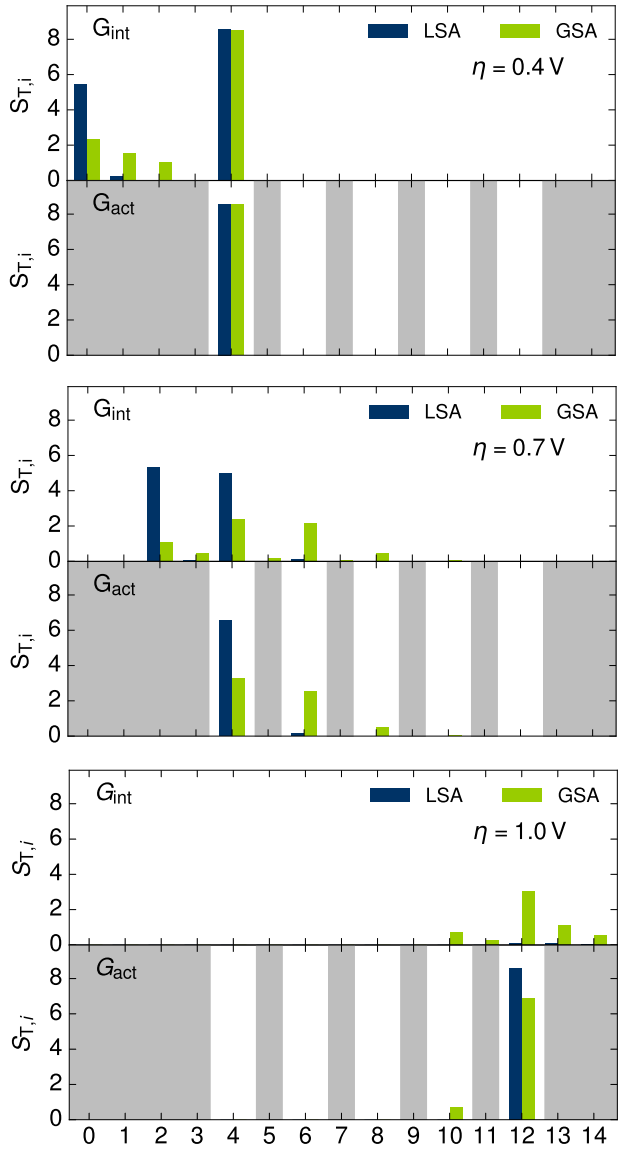

FIG. 5. Local and global sensitivity indices $S_{\mathrm{T},i}$ for the 20 input parameters for the (110-A) structure of the oxygen evolution reaction at three different overpotentials $\eta \in \{0.4, 0.7, 1.0\}$ V. The gray-shaded fields describe intermediate states that are not considered for a reaction in the model (see the text). Shown are the sensitivities of $\log_{10}(\mathrm{TOF} \times \mathrm{s})$ with respect to the errors in $G_{\mathrm{int},i}$ and $G_{\mathrm{act},i}$.

are thermodynamically unfavorable. The reaction {1} therefore happens from the state with the lowest possible degree of oxidation, A_4. Within the range of values examined in the sensitivity analysis, the free energies of the states with higher degrees of oxidation never become low enough to result in a significant probability for the surface to exist in these states. As a result, the kinetics are always controlled by the states with low degrees of oxidation over the entire range of parameter space explored in the sensitivity analysis at this applied overpotential.

At higher applied overpotentials, states with higher degrees of oxidation begin to dominate the probability distribution [cf. Eq. (3)]. Under these conditions, the surface does not have a significant probability of occurring in states with lower degrees of oxidation so that the free energies associated with these states do not have any influence on the kinetics.

Besides this common trend captured by both the LSA and GSA, we also find notable differences. Most noticeably, LSA assigns zero significance to many important energies, as identified by the TSI. For $\eta = 0.4$ V, LSA returns non-vanishing sensitivities for four energies, whereas GSA finds non-zero sensitivities for five parameters. For the applied overpotential of $\eta = 0.7$ V, LSA identifies only three energies with non-vanishing sensitivities. GSA instead shows that there are nine energies with non-vanishing TSIs, of which eight have a TSI around 0.5 or above. At the highest applied overpotential of $\eta = 1.0$ V, the LSA identifies only one energy with non-vanishing sensitivity, while the GSA identifies seven such energies.

The origin of the non-linearities leading to the discrepancies between the LSA and GSA can be traced to the non-linear form of the equation for the TOF, which can be expressed as

$$\mathrm{TOF} = \frac{k_\mathrm{B}T}{h}\frac{\sum_i \exp\left(-\frac{G_{\mathrm{act},i} + G_{\mathrm{int},i} - n_i e\eta}{k_\mathrm{B}T}\right)}{\sum_j \exp\left(-\frac{G_{\mathrm{int},j} - n_j e\eta}{k_\mathrm{B}T}\right)}, \tag{22}$$

using Eqs. (1)–(3). At most values of η, one exponential term will dominate each of the sums in the numerator and denominator so that the logarithm of the TOF will approximately resemble a piecewise-linear function,

$$\log_{10}\mathrm{TOF} \approx \log_{10}\left(\frac{k_\mathrm{B}T}{h}\right) - \frac{\log_{10} e_\mathrm{Euler}}{k_\mathrm{B}T}(G_{\mathrm{act},i} + G_{\mathrm{int},i} - G_{\mathrm{int},j}) + \frac{\log_{10} e_\mathrm{Euler}}{k_\mathrm{B}T}(n_i - n_j)e\eta, \tag{23}$$

where e_Euler is Euler's number, in Eq. (23), i corresponds to the transition state with the lowest free energy $G_{\mathrm{act},i} + G_{\mathrm{int},i} - n_i e\eta$, and j corresponds to the intermediate state with the lowest free energy $G_{\mathrm{int},j} - n_j e\eta$. From this analysis, we can see that as long as the uncertainty window lies within a single linear kinetic regime [i.e., i and j in Eq. (23) do not change], LSA and GSA should give identical results. In this situation, both methods would predict non-vanishing sensitivities for $G_{\mathrm{act},i}$, $G_{\mathrm{int},i}$, and $G_{\mathrm{int},j}$. If the uncertainty window encompasses multiple linear kinetic regimes, however, the GSA will predict non-vanishing sensitivities for the energies $G_{\mathrm{act},i}$, $G_{\mathrm{int},i}$, and $G_{\mathrm{int},j}$ in all of the these kinetic regimes. By contrast, the LSA will only indicate non-vanishing sensitivities for those energy parameters corresponding to the kinetic regime in which the nominal values lie. At $\eta = 0.4$ V, these correspond to $i = 0$ and $j = 4$, at $\eta = 0.7$ V $i = 2$ and $j = 4$, and at $\eta = 1.0$ V $i = j = 12$. For this last value of η, we note that the LSA indicates no significant sensitivity with respect to any of the intermediate states because $i = j$, and therefore $G_{\mathrm{int},i} - G_{\mathrm{int},j} = 0$ in Eq. (23).

Additionally, even when the LSA correctly identifies the energies with non-vanishing sensitivities, it tends to overestimate these sensitivities. This is due to the fact that LSA falsely assumes that these energies have high sensitivities over the entire range of uncertainty. By contrast, the GSA correctly captures transitions to different linear kinetic regimes at large enough deviations from the nominal values, which is associated with a shift in sensitivity towards different energies of different states. At $\eta = 0.4$ V, this concerns only $G_{\mathrm{int},0}$. $G_{\mathrm{int},4}$ and $G_{\mathrm{act},4}$ are accurately estimated by the LSA because the reaction occurs predominantly through the state with $j = 4$ over the entire uncertainty window. At $\eta = 0.7$ V, all three relevant sensitivities (according to LSA) are overestimated and we have a shift of the sensitivity to states with higher degrees of oxidation. For the highest overpotential $\eta = 1$ V, the sensitivity of the single important parameter from LSA is only slightly overestimated. Again, this is due to the fact that the reaction occurs predominantly through a single state ($j = 12$) over the entire uncertainty window.

It should be noted that while a linear $f(x)$ implies an agreement between LSA and GSA for the sensitivities, the opposite argument is not valid. Whether the function is approximately linear can be seen however from the SG expansion. If the function is linear, the surplus of all BFs $\varphi_{\vec{l},\vec{i}}$ with $|\vec{l}|_1 > 1$ should vanish and the surplus of the two BFs within one level $\vec{l}$, $|\vec{l}|_1 = 1$ must add to zero.

The above reasoning qualitatively explains why GSA predicts potentially more non-zero sensitivities than LSA and why important energies according to LSA tend to have too large sensitivities. Now, this explanation still allows for two interpretations: (i) the one-dimensional functions in the ANOVA decomposition are non-linear or (ii) there are additional interactions between the parameters. If only (i) is the case, we would have a perfect variance decomposition and we could reconstruct the function from one-dimensional scans along each axis. The disagreement from a linear behavior must then directly appear in these scans. If we have additional interactions, this simple procedure will not provide the full information and may even be misleading. The function might behave linearly along the axes while globally being strongly non-linear.

In order to get an idea of the important non-linear interactions, we have calculated the first order indices

$$V_i = V(E_{X_{\sim i}}(Y|X_i)) \tag{24}$$

and the second order indices

$$V_{ij} = V(E_{X_{\sim ij}}(Y|X_i, X_j)) - V_i - V_j \tag{25}$$

for the case $\eta = 0.7$ V, as this overpotential leads to the most complex sensitivity pattern. Performing the respective sums, we find that first order effects account for roughly 65%–70% of the total variance, while second order effects are responsible for ≈25%. About 5%–10% are due to higher order couplings. The function therefore has an intrinsic multidimensional character.

The second order index is depicted in Fig. 6 but only for parameters with non-vanishing TSI, as V_{ij} is never larger than $\min(S_{\mathrm{T},i}, S_{\mathrm{T},j})$. We find the strongest couplings between pairs, where one partner is one of the activation energies $G_{\mathrm{act},4}$ or $G_{\mathrm{act},6}$. Each activation energy interacts strongest with the corresponding intermediate energies. For the intermediate states 2, 3, and 5, which do not allow for the reaction in the considered model, the intermediate energies couple only with other intermediate energies but not with the activation energies. The reason for this can be seen from taking the logarithm of Eq. (22),

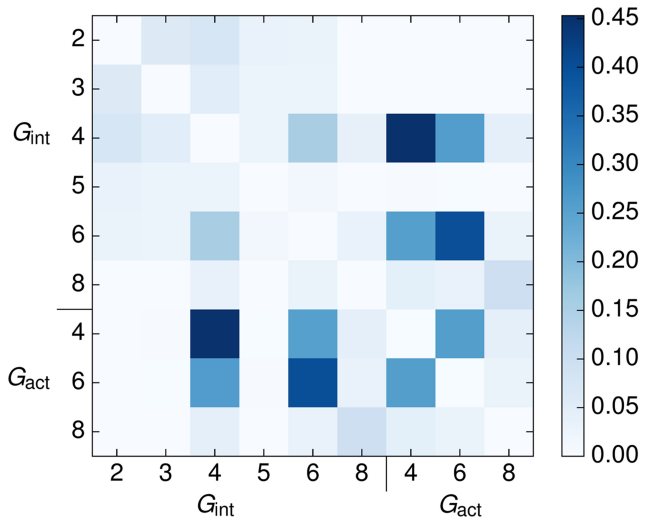

FIG. 6. Second order indices with respect to the input parameters of the OER model on the (110)-A surface for an overpotential of $\eta = 0.7$ V.

$$\log_{10}\text{TOF} = -\log_{10}\left(\sum_{j=0}^{14}\exp\left(-\frac{G_{\text{int},j} - je\eta}{kT}\right)\right) + \log_{10}\left(\sum_{j=2}^{6}\exp\left(-\frac{G_{\text{act},2j} + G_{\text{int},2j} - je\eta}{kT}\right)\right) + \log_{10}\left(\frac{kT}{h}\right). \quad (26)$$

The first term does not depend on the activation energies and the second term does not depend on $G_{\text{int},2}$, $G_{\text{int},3}$, and $G_{\text{int},5}$. The second order indices between elements of these two classes must then be zero.

B. Discussion

The uncertainty analysis illustrates the potential impact of the approximate DFT energetics in microkinetic modeling. One of the key objectives of such modeling, the TOF, might carry an uncertainty of several orders of magnitude such that a qualified statement cannot be made on the question whether the surface is highly active or not. We have also found this in a previous study on the first-principles kinetic Monte Carlo model for the CO oxidation on $RuO_2(110)$.[10]

However, the global sensitivity analysis discussed in Sec. V A reveals that it is still possible to identify the key atomistic aspects controlling the reactivity—even if one assumes only the worst case scenario and a corresponding PDF. For each overpotential, only a fraction of all energetic errors has an influence on the model outcome, i.e., variation of the respective parameters results in a potentially larger variation of the TOF than variations of the others. In a more kinetic language, we would therefore assign the adjective "kinetically relevant" to those parameters with high sensitivity indices. These important errors belong to only very few intermediate states. We can conclude that the physical details of these states potentially control the reactivity, irrespective of the possible error. Our results indicate that these kinetically relevant states change with the applied overpotential. Thus, an identification of one or two atomistic indicators that control the reactivity at all reasonable overpotentials is generally not possible.

The devised locally and dimension-adaptive SG approach performs well for carrying out the GSA, requiring only a modest number of function evaluations to achieve a high accuracy. For the problem at hand, this is not so crucial, as even millions of function evaluations would come at negligible costs compared to the underlying DFT calculations. By contrast, for complex models like kinetic Monte Carlo simulations, the number of function evaluations might become a major issue. The case $\eta = 0.7$ V requires generally more points to achieve a target threshold *tol*. As detailed in Sec. V A, the system has a higher intrinsic dimensionality at this overpotential than at the other two, i.e., the number of non-vanishing TSIs is larger. It is this intrinsic dimensionality which matters more for the convergence behavior of a dimension-adaptive SG approach than the true dimensionality.

A problem with the adaptive SG approach is the need for a sufficiently resolved initial grid. Only then, the adaptive strategy accurately explores the parameter space and does not terminate prematurely. Here, we addressed this by imposing an extremely high threshold and restricting the maximum resolution in an initial phase. For complex models, this might not be appropriate, as the required high accuracy in the model evaluations may not be affordable. Overcoming this limitation will be a subject of our future research.

Besides the presence of large uncertainties in the predicted TOF, our results demonstrate that the mere use of LSA might lead to erroneous conclusions about the most important uncertainties. As discussed in Sec. V A, LSA might fail to identify all errors which have an impact, as seen most prominently for the overpotential $\eta = 0.7$ V. Furthermore, it overestimates the sensitivities with respect to other parameters. This failure of LSA becomes critical when we want to employ sensitivity analysis to identify parameters which should be calculated with higher accuracy. Because LSA might miss some important parameters, we would identify very few energies for higher-level treatment if we only consider LSA and the corresponding equation for the variance, Eq. (8). Also, after refinement of the identified parameters at a higher level of theory, the latter might then give an artificially low estimate of the variance for the model, leading us to falsely conclude that our refined model is accurate enough. For instance, let us consider the case with $\eta = 0.7$ V and suppose we have a method with which we can achieve an accuracy of 0.06 eV, i.e., a factor five better than our employed accuracy of 0.3 eV. Of course, such a method would likely be significantly more expensive than a semi-local DFT calculation and we would like to employ it for only those energies which are most important. If we now only consider the LSA results from the middle panel of Fig. 5, the only three energies with non-vanishing sensitivities are $G_{\text{int},2}$, $G_{\text{int},4}$, and $G_{\text{act},4}$, and the LSA estimated variance is 17.2. After improving these energies, the LSA estimate of the variance would be 1, where, for simplicity, we assumed that the new nominal energy values agree with the old ones. If we now calculate the true (GSA) variance, we have 9.5 before improving the three energies and 4.6 afterwards. Instead of a variance reduction by a factor 17, as LSA implies, we achieved only at reduction by a factor 2 in reality. That is, we improve the accuracy of the TOF

by a factor of eight, instead of the more than three orders of magnitude suggested by the misleading linear approximation. If we now improve the four most important energies according to the GSA from middle panel of Fig. 5, the resulting variance is 3, i.e., the accuracy of the TOF was improved by a factor of 22. But unlike LSA, GSA suggests how to proceed further. Reducing the error of all nine energies with non-vanishing sensitivities results in a variance of 0.6 and we achieved the targeted large reduction.

The simple example discussed above illustrates that resources only need to be spent on refining those parameters with a high sensitivity index. GSA therefore might serve as an ingredient to a hierarchical modeling strategy, where one exploits methods with increasing accuracy for computing the energetics. In the first step of a hierarchical parameter estimation, the energetics are determined with the cheapest but also most inaccurate method. After a GSA, only the most important parameters will be improved using the method having the next highest accuracy. A new GSA with an updated PDF will then reveal which parameters to improve next. This is repeated until one either achieves a target accuracy or further improvement would become too computationally expensive. In such an approach, one may want to include approaches which are even less accurate than semi-local DFT (and computationally also less expensive). The value of a mere LSA is then even more questionable, as with the larger error bounds, the importance of non-linearities also increases.

In principle, GSA is performed to quantify the parametric dependence of a given model on its input parameters. Now, reduced kinetic models are often only reasonable for a certain set of parameters. The question then arises whether the sensitivities determined for such a reduced model are robust against the extension of the model. For the OER on Co_3O_4 (110)-A, a straightforward extension would be the inclusion of reaction {1} from odd-numbered intermediate states. These have been excluded in the original model because the corresponding intermediate states are not populated at the nominal settings.[29,30] If we allow to vary the energies of the intermediates, as is done during the GSA, this may no longer be the case.

In Fig. 7, we have calculated the local and global sensitivity indices for $\eta = 0.7$ V, where we have included reaction {1} from the odd-numbered states 5–11 (the states below 4 do not allow for reaction {1}). For simplicity, we have set the nominal barriers to 0.6 eV as all other barriers are close to this value. As expected, the LSA results hardly change compared to the original model (cf. the middle panel of Fig. 5). For GSA, the situation is very different. The sensitivities for the even states up to 6 hardly change, but now the intermediate energies for the odd states 5, 7, and 9 are also important, unlike in the original model in Fig. 5. Concomitantly, the corresponding newly introduced activation barriers also show finite sensitivities. Additionally, the sensitivity with respect to the energy parameters of intermediate state 8 changes: While in the original model it had only a minor impact, the corresponding $S_{T,i}$ are now sizable. The rise in importance for the odd-numbered intermediate states 5, 7, and 9 could have been expected from the GSA of the original model. At $\eta = 0.7$ V, these states are close in free energy (and charge) to the even states that do

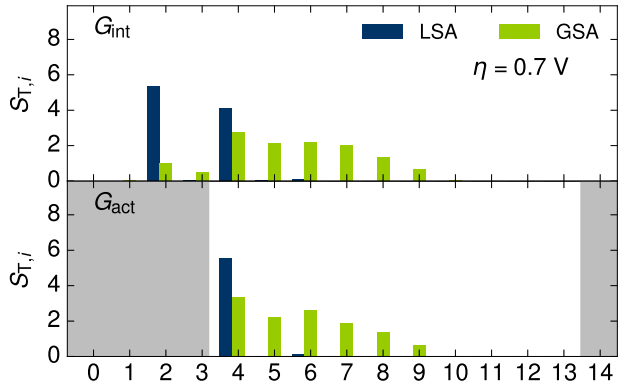

FIG. 7. Local and global sensitivity indices $S_{T,i}$ for the extended model of the OER on the (110)-A surface for an overpotential $\eta = 0.7$ V. The gray-shaded fields describe intermediate states that are not considered for a reaction in the model (see the text). Shown are the sensitivities of $\log_{10}(\text{TOF} \times \text{s})$ with respect to the errors in the input parameters.

show finite sensitivity in the original model. Because of this predictable structure, GSA might actually guide chemical intuition in the extension of a coarser model. For the OER on the (110)-A surface, GSA suggests to only add the intermediate states 5 and 7 in a first step, and, indeed, this largely resembles the full case in Fig. 7 (cf. the supplementary material).

While in the original model there are only eight parameters with significant TSI, the extended model shows a sensitivity above 0.5 with respect to more than fourteen parameters. This higher intrinsic dimensionality has a significant impact on the performance of the adaptive SG methodology. While we needed only ≈14 000 grid points for a threshold $tol = 0.001$, approximately 70 000 grid points were needed for the extended model and a threshold of $tol = 0.01$.

It is important to note that the results of our sensitivity analysis depend on our choice of the error model, and we have employed a rather generous PDF which only imposes the bound constraints on the errors of the individual parameters. In reality, we expect that the DFT errors of different parameters are correlated. For the system at hand, the errors in the free energies of the intermediate states most likely arise from an inaccurate description of the oxidation of Co(III) to Co(IV) by the DFT + U method. We therefore expect that the intermediate energies tend to be strongly correlated (either being all over- or underestimated) and not independent as we have assumed. Also the barriers have very close values, which suggests that these might be independent of the actual degree of oxidation and the errors would essentially be the same for all barriers. Finally, the Bronsted-Evans-Polanyi theory implies that these barriers are not completely independent of the corresponding intermediate energies. A corresponding correlated PDF would then lead to a different uncertainty, and we would expect that this uncertainty is lower than for the employed uncorrelated PDF. Of course, also the sensitivities might change as well as the first and second order indices, for which we would need to consider a generalized version of ANOVA for dependent parameters.[41] But these changes, especially the relative changes, are largely unpredictable because they depend on the details of the correlated PDF. However, a GSA with a rather simple PDF, like the one employed, might serve as a starting point for the identification of which parameter correlations

should be investigated in more detail, e.g., using the methodologies outlined in Refs. 9 and 39. Such an improvement of the PDF might also be incorporated in the hierarchical model construction outlined above. That is, we first determine the correlations between parameters on the lower level and see how this changes the sensitivities. Based on this information, we then proceed with improving the important parameters with a higher level method.

Another potential application of GSA would be in the context of computational materials screening,[38] where parameter uncertainty arises due to the desire to inexpensively examine a large class of materials. GSA and SGs might serve here as a tool to identify indicators of the catalytic function which can be computed economically. Also different parametrizations of the problem—e.g., linear scaling relations,[38] UBI-QEP,[47] or from some machine learning procedure[48,49]—could be compared and one could choose the parametrization for which inclusion of the expensive parameters has a small enough impact that their calculation can be avoided.

VI. CONCLUSION

We have presented an approach to quantify the impact of individual errors in the input parameters on the response of a first-principles microkinetic model. The approach utilizes locally and dimension-adaptive sparse grids for the determination of variance-based global sensitivity measures. This allows the efficient numerical quadrature of the high-dimensional integrals required for global sensitivity analysis. Due to the possibility to work with only relatively few model evaluations, more complex models might become tractable, such as kinetic Monte Carlo[50] or other methods addressing the direct solution of the master equation.[51,52] As one might expect, the method's performance diminishes when the exploited properties—like low intrinsic dimensionality—are not so pronounced. Our future work will concentrate on improving the adaptive strategy, on application of the mentioned complex models, and on the comparison with other approaches to GSA.[8,10,53]

We tested our approach on a model for the electrochemical oxygen evolution reaction on the Co_3O_4 (110)-A surface at room temperature. For the employed error model, we find a sizable uncertainty for the predicted turnover frequency, up to the level that makes it impossible to assess whether the catalyst is active or not. We want to emphasize that our results depend on the employed parametrization and error model. Both were chosen to pose a challenging test case; in reality, however, existing correlations might reduce the uncertainty to an acceptable level. Not withstanding, even with the here employed error model, our global sensitivity analysis reveals that it is still possible to identify the key atomistic aspects driving or hindering the catalytic performance. However, the commonly used local sensitivity analysis appears inadequate to identify these parameters due to strong non-linearities in the response of the model when varying the parameters within the typical error bounds.

Our approach might ultimately aid in the construction of kinetic models from first principles by identifying those kinetic parameters which should be investigated more deeply, either by some higher-level electronic structure method[11,12] or by incorporating previously ignored aspects, e.g., solvation effects.[54] The outlined methodology might also be of help in the context of materials screening, where it could serve as a tool to identify suitable indicators for catalytic performance.

SUPPLEMENTARY MATERIAL

See supplementary material for convergence tests, for an alternative representation of the uncertainty, and for the GSA for an extended model with reactions only enabled for the intermediate states 5 and 7.

ACKNOWLEDGMENTS

This research was carried out in the framework of Matheon, Project Nos. SE14 and SE23, supported by Einstein Foundation Berlin. C.P. acknowledges partial support from the Solar Technologies Go Hybrid initiative of the State of Bavaria.

[1] M. K. Sabbe, M.-F. Reyniers, and K. Reuter, Catal. Sci. Technol. **2**, 2010 (2012).
[2] M. Saeys, M.-F. Reyniers, M. Neurock, and G. B. Marin, J. Phys. Chem. B **109**, 2064 (2005).
[3] O. R. Inderwildi, S. J. Jenkins, and D. A. King, J. Phys. Chem. C **112**, 1305 (2008).
[4] A. A. Gokhale, J. A. Dumesic, and M. Mavrikakis, J. Am. Chem. Soc. **130**, 1402 (2008).
[5] K. S. Exner, F. Heß, H. Over, and A. P. Seitsonen, Surf. Sci. **640**, 165 (2015).
[6] S. Matera, S. Blomberg, M. J. Hoffmann, J. Zetterberg, J. Gustafson, E. Lundgren, and K. Reuter, ACS Catal. **5**, 4514 (2015).
[7] A. J. Medford, J. Wellendorff, A. Vojvodic, F. Studt, F. Abild-Pedersen, K. W. Jacobsen, T. Bligaard, and J. K. Nørskov, Science **345**, 197 (2014).
[8] J. E. Sutton, W. Guo, M. A. Katsoulakis, and D. G. Vlachos, Nat. Chem. **8**, 331 (2016).
[9] E. Walker, S. C. Ammal, G. A. Terejanu, and A. Heyden, J. Phys. Chem. C **120**, 10328 (2016).
[10] S. Döpking and S. Matera, Chem. Phys. Lett. **674**, 28–32 (2017).
[11] A. Kubas, D. Berger, H. Oberhofer, D. Maganas, K. Reuter, and F. Neese, J. Phys. Chem. Lett. **7**, 4207 (2016).
[12] C. P. Plaisance, R. A. van Santen, and K. Reuter, J. Chem. Theory Comput. **13**, 3561 (2017).
[13] C. T. Campbell, Top. Catal. **1**, 353 (1994).
[14] *Compendium of Chemical Terminology (the "Gold Book")*, 2nd ed. compiled by A. D. McNaught and A. Wilkinson, online version by M. Nic, J. Jirat, and B. Kosata, updates by A. Jenkins (IUPAC, 1997/2006-).
[15] H. Meskine, S. Matera, M. Scheffler, K. Reuter, and H. Metiu, Surf. Sci. **603**, 1724 (2009).
[16] M. J. Hoffmann, F. Engelmann, and S. Matera, J. Chem. Phys. **146**, 044118 (2017).
[17] H.-J. Bungartz and M. Griebel, Acta Numer. **13**, 147 (2004).
[18] A. Saltelli, M. Ratto, T. Andres, F. Campolongo, J. Cariboni, D. Gatelli, M. Saisana, and S. Tarantola, *Global Sensitivity Analysis. The Primer* (Wiley VCH Verlag, 2008).
[19] G. E. B. Archer, A. Saltelli, and I. M. Sobol, J. Stat. Comput. Simul. **58**, 99 (1997).
[20] K. Reuter, Catal. Lett. **146**, 541 (2016).
[21] F. Nobile, R. Tempone, and C. G. Webster, SIAM J. Numer. Anal. **46**, 2309 (2008).
[22] X. Ma and N. Zabaras, J. Comput. Phys. **229**, 3884 (2010).
[23] J. D. Jakeman and S. G. Roberts, *Sparse Grids and Applications* (Springer, 2012), pp. 181–203.
[24] E. Plischke, E. Borgonovo, and C. L. Smith, Eur. J. Oper. Res. **226**, 536 (2013).
[25] D. Strobusch and C. Scheurer, J. Chem. Phys. **140**, 074111 (2014).
[26] M. Griebel, Computing **61**, 151 (1998).
[27] D. Pflüger, *Spatially Adaptive Sparse Grids for Higher-Dimensional Problems* (Verlag Dr. Hut, 2010).
[28] J. D. Jakeman and S. G. Roberts, preprint arXiv:1110.0010 (2011).

[29]C. P. Plaisance and R. A. van Santen, J. Am. Chem. Soc. **137**, 14660 (2015).
[30]C. P. Plaisance, K. Reuter, and R. A. van Santen, Faraday Discuss. **188**, 199–226 (2016).
[31]M. G. Walter, E. L. Warren, J. R. McKone, S. W. Boettcher, Q. Mi, E. A. Santori, and N. S. Lewis, Chem. Rev. **110**, 6446 (2010).
[32]A. Marshall, B. Børresen, G. Hagen, M. Tsypkin, and R. Tunold, Energy **32**, 431 (2007).
[33]A. Roudgar, M. Eikerling, and R. van Santen, Phys. Chem. Chem. Phys. **12**, 614 (2010).
[34]V. I. Anisimov and O. Gunnarsson, Phys. Rev. B **43**, 7570 (1991).
[35]A. I. Liechtenstein, V. I. Anisimov, and J. Zaanen, Phys. Rev. B **52**, R5467 (1995).
[36]V. I. Anisimov, F. Aryasetiawan, and A. I. Lichtenstein, J. Phys.: Condens. Matter **9**, 767 (1997).
[37]A. J. Cohen, P. Mori-Sanchez, and W. Yang, Science **321**, 792 (2008).
[38]J. K. Nørskov, T. Bligaard, J. Rossmeisl, and C. H. Christensen, Nat. Chem. **1**, 37 (2009).
[39]J. Wellendorff, K. T. Lundgaard, A. Møgelhøj, V. Petzold, D. D. Landis, J. K. Nørskov, T. Bligaard, and K. W. Jacobsen, Phys. Rev. B **85**, 235149 (2012).
[40]S. Kucherenko, S. Tarantola, and P. Annoni, Comput. Phys. Commun. **183**, 937 (2012).
[41]S. Rahman, SIAM/ASA J. Uncertainty Quantif. **2**, 670 (2014).
[42]T. Homma and A. Saltelli, Reliab. Eng. Syst. Saf. **52**, 1 (1996).
[43]T. Gerstner and M. Griebel, Computing **71**, 65 (2003).
[44]H. Yserentant, Computing **78**, 195 (2006).
[45]A. Klimke and B. Wohlmuth, ACM Trans. Math. Software **31**, 561 (2005).
[46]M. Griebel and M. Holtz, J. Complexity **26**, 455 (2010).
[47]E. Shustorovich and H. Sellers, Surf. Sci. Rep. **31**, 1 (1998).
[48]Z. W. Ulissi, A. J. Medford, T. Bligaard, and J. K. Nørskov, Nat. Commun. **8**, 14621 (2017).
[49]L. M. Ghiringhelli, J. Vybiral, E. Ahmetcik, R. Ouyang, S. V. Levchenko, C. Draxl, and M. Scheffler, New J. Phys. **19**, 023017 (2017).
[50]M. Stamatakis and D. G. Vlachos, ACS Catal. **2**, 2648 (2012).
[51]G. J. Herschlag, S. Mitran, and G. Lin, J. Chem. Phys. **142**, 234703 (2015).
[52]P. Gelß, S. Matera, and C. Schütte, J. Comput. Phys. **314**, 489 (2016).
[53]A. Alexanderian, F. Rizzi, M. Rathinam, O. P. Le Maître, and O. M. Knio, J. Sci. Comput. **58**, 592 (2014).
[54]S. Ringe, H. Oberhofer, C. Hille, S. Matera, and K. Reuter, J. Chem. Theory Comput. **12**, 4052 (2016).